


Visibility of Prominences Using the He I D₃ Line Filter on the PROBA-3/ASPIICS Coronagraph

S. Ježič^{1,2}  · P. Heinzel² · N. Labrosse³ ·
A.N. Zhukov^{4,5} · A. Bemporad⁶ · S. Fineschi⁶ · S. Gunár²

Received: 20 June 2017 / Accepted: 24 January 2018 / Published online: 5 February 2018
© Springer Science+Business Media B.V., part of Springer Nature 2018

Abstract We determine the optimal width and shape of the narrow-band filter centered on the He I D₃ line for prominence and coronal mass ejection (CME) observations with the ASPIICS (*Association of Spacecraft for Polarimetric and Imaging Investigation of the Corona of the Sun*) coronagraph onboard the PROBA-3 (*Project for On-board Autonomy*) satellite, to be launched in 2020. We analyze He I D₃ line intensities for three representative non-local thermal equilibrium prominence models at temperatures 8, 30, and 100 kK computed with a radiative transfer code and the prominence visible-light (VL) emission due to Thomson scattering on the prominence electrons. We compute various useful relations at prominence line-of-sight velocities of 0, 100, and 300 km s⁻¹ for 20 Å wide flat filter and

✉ S. Ježič
sonja.jejcic@guest.arnes.si

P. Heinzel
pheinzel@asu.cas.cz

N. Labrosse
nicolas.labrosse@glasgow.ac.uk

A.N. Zhukov
andrei.zhukov@sidc.be

A. Bemporad
bemporad1@oato.inaf.it

S. Fineschi
fineschi@oato.inaf.it

S. Gunár
stanislav.gunar@asu.cas.cz

¹ Faculty of Mathematics and Physics, University of Ljubljana, Ljubljana, Slovenia

² Astronomical Institute of the Czech Academy of Sciences, Ondřejov, Czech Republic

³ SUPA School of Physics & Astronomy, University of Glasgow, Glasgow, UK

⁴ Solar-Terrestrial Centre of Excellence-SIDC, Royal Observatory of Belgium, Brussels, Belgium

⁵ Skobel'syn Institute of Nuclear Physics, Moscow State University, Moscow, Russia

⁶ INAF-Turin Astrophysical Observatory, Pino Torinese (TO), Torino, Italy

three Gaussian filters with a full-width at half-maximum (FWHM) equal to 5, 10, and 20 Å to show the relative brightness contribution of the He I D₃ line and the prominence VL to the visibility in a given narrow-band filter. We also discuss possible signal contamination by Na I D₁ and D₂ lines, which otherwise may be useful to detect comets. Our results mainly show that i) an optimal narrow-band filter should be flat or somewhere between flat and Gaussian with an FWHM of 20 Å in order to detect fast-moving prominence structures, ii) the maximum emission in the He I D₃ line is at 30 kK and the minimal at 100 kK, and iii) the ratio of emission in the He I D₃ line to the VL emission can provide a useful diagnostic for the temperature of prominence structures. This ratio is up to 10 for hot prominence structures, up to 100 for cool structures, and up to 1000 for warm structures.

Keywords Instrumentation and data management · Prominences, models

1. Introduction

Coronagraphic observations of the Sun from space have been limited so far in that only the outer corona has been detected. Instruments such as the *Large Angle and Spectrometric Coronagraph* (LASCO) or the *Ultraviolet Coronagraph Spectrometer* (UVCS) onboard the *Solar and Heliospheric Observatory* (SOHO) (Brueckner *et al.*, 1995; Kohl *et al.*, 1995), or COR2 coronagraphs on the twin *Solar Terrestrial Relations Observatory* (STEREO) satellites (Howard *et al.*, 2008) used external occulters that are placed in front of the telescopes, which resulted in occultation that significantly exceeded the solar disk radius. This was dictated by the amount of stray light. We note that stray light is high in internally occulted coronagraphs such as STEREO/COR1. However, by placing the external occulting disk farther from the telescope itself, stray light can be gradually reduced and lower coronal altitudes may be reached, which enables studying the innermost corona. This type of experiment is designed for the upcoming mission *Project for On-board Autonomy* (PROBA-3) of the European Space Agency (ESA). PROBA-3 is a technology-demonstration mission within ESA's General Support Technology Programme (GSTP), aimed at testing the so-called 'formation flight of two satellites' (launch is expected in 2020). The two satellites, separated on their orbits by about 150 meters, will carry a large externally occulted coronagraph, where the occulter will be placed on the front satellite oriented toward the Sun and the telescope will be on the rear satellite. This coronagraph, called ASPIICS (*Association of Spacecraft for Polarimetric and Imaging Investigation of the Corona of the Sun*) (Lamy *et al.*, 2010; Renotte *et al.*, 2016) will then be precisely oriented in space in order to observe the Sun, and this orientation will fulfill part of the formation-flight tests. With this configuration, the inner corona down to 1.08 solar radii (*i.e.* about 60 Mm above the limb) can be observed with unprecedented imaging quality. In a sense, this will simulate a total solar eclipses, with the advantage of obtaining extended time series of coronal images, which will allow us for the first time to study the evolution and dynamics of the inner corona on timescales reaching six hours.

One of the science objectives is also the observation of eruptive prominences and coronal mass ejections (CMEs) in the field of view (FOV) of ASPIICS, using filter imaging techniques. The filter wheel is still under design study, and it is the main objective of this paper to propose its transmittance properties. We use our previous experience with the He I D₃ line emission in cool prominence-like structures (Labrosse, 2015) and study their expected visibility through the ASPIICS coronagraph. This visibility critically depends on the physical conditions in eruptive prominences and cores of CMEs, as well as on their velocities in

the corona, and it depends on the transmittance profile of the narrow-band He I D₃ filter. We also discuss a potential contamination of the signal by prominence emission in the nearby sodium doublet Na I D₁ and D₂. The point is that if the filter is wide enough, the latter lines can be well detected in comets passing through the ASPIICS FOV. Images acquired by space-based coronagraphs have proven to be very useful for observations of near-Sun comets and even Sun-grazing (Biesecker *et al.*, 2002) and Sun-skirting (Lamy *et al.*, 2013) comets. These comets have been observed in the visible-light (VL) even by the STEREO coronagraphs (Thompson, 2009), and a few of them have also been observed in UV spectra (Bemporad *et al.*, 2007) and extreme ultraviolet (EUV) images (McCauley *et al.*, 2013). All these observations provided much information about the origin and evolution of these small bodies in our solar system (Sekanina, 2003).

While this paper is aimed at proposing the narrow-band filter transmittance characteristics for the He I D₃ line, in a following paper we will focus on the diagnostic potential of this He I D₃ line, combined with VL, and this will serve for the future analysis of the ASPIICS data. Broad-band data of this type already exist for structures at higher altitudes. The LASCO-C2 coronagraph on SOHO has several broad-band filters, one of them centered on the He I D₃ lines (the so-called orange filter). Several observations of prominence-like structures with this orange filter exist in the literature (Boulade *et al.*, 1997), and the question thus arises whether the image is dominated by the He I D₃ line or by VL integrated through the broad-band filter. The latter is due to Thomson scattering on electrons, which are part of the erupting structure (the coronal component subtracted). The optimum parameters of the He I D₃ filter, contamination with the sodium D₁ and D₂ lines, and the comet detection capability with the ASPIICS coronagraph are the main objectives of this article.

2. Narrow-Band Filter Observations of the Neutral Helium He I D₃ Line

The ASPIICS coronagraph onboard the PROBA-3 satellite will carry a filter wheel with a total of six filter slots: a broad-band VL filter between 5400 and 5700 Å, three VL polarizers at angles 0 and ±60°, an iron Fe XIV green-line narrow-band 5 Å filter, and finally one narrow-band filter to detect plasmas in the neutral helium He I D₃ at 5877.25 Å (we use the vacuum wavelength). The design of the He I D₃ narrow-band filter is still in progress.

The narrow-band filter centered on the He I D₃ line contains the radiation contribution from four sources: i) prominence emission in the He I D₃ line, which is mainly due to scattering of the photospheric radiation on prominence helium atoms, ii) VL emission due to Thomson scattering on prominence electrons, iii) VL emission from the surrounding corona along the line-of-sight (LOS) due to Thomson scattering on coronal electrons, and iv) coronal He I D₃ line emission. Here we do not consider iii) because the LOS contribution of the surrounding corona can be subtracted using the nearby pre-eruption coronal observation and iv), which is below the detection limit because coronal temperatures are much higher than the formation temperature of the He I D₃ line.

We focus on three types of Gaussian filters with an FWHM equal to 5, 10, and 20 Å to study the relative brightness contribution of the He I D₃ line and the prominence VL to the visibility in a given filter. We also take into account the possible contamination with the nearby sodium Na I D₁ and D₂ lines at 5897.56 and 5891.58 Å. The advantage of the ASPIICS coronagraph on PROBA-3 is to have nearly simultaneous narrow-band He I D₃ line and broad-band VL observations for the whole FOV down to 1.08 R_☉ with strongly reduced stray light. Since ASPIICS will not provide spectroscopic He I D₃ observation, however, there will be no information about the prominence LOS velocity. Without such

information, we cannot quantitatively interpret the prominence He I D₃ emission unless the He I D₃ narrow-band filter has a flat response function in the wavelength range corresponding to the expected Doppler shifts. In the present work we compare the effect of the prominence LOS velocity for three Gaussian filters with different FWHMs against the reference 20 Å wide flat filter.

3. Modeling of the Prominence Emission in the He I D₃ Line

The emerging intensities in the He I D₃ line are computed using the non-LTE (*i.e.* departures from local thermodynamic equilibrium, LTE) radiative-transfer code presented in Labrosse and Gouttebroze (2001) for a grid of prominence models. The code solves the pressure-balance and ionization equilibrium equations, as well as radiative-transfer and statistical equilibrium equations for hydrogen in a one-dimensional (1D) plane-parallel slab standing vertically above the solar surface. When these equations are solved, radiative-transfer and statistical equilibrium equations are solved for a 34-level helium atom model, with 29 levels for He I, four levels for He II, and one continuum level for fully ionized helium. This allows us to obtain the emerging intensities as a function of model input parameters. The input parameters are temperature, gas pressure, microturbulent velocity, radial flow velocity, slab thickness, and altitude above the limb. The slab is externally illuminated by the solar disk. For this exploratory study, we focus on isothermal and isobaric prominence slabs at three altitudes above the limb (60 Mm, 800 Mm, and 1600 Mm, which roughly corresponds to 1.08 R_{\odot} , 2.15 R_{\odot} , and 3 R_{\odot}) that are representative of what might be observed with the ASPIICS coronagraph. We computed a total of 90 models with temperatures ranging from 8 kK to 100 kK, with a thickness of 1000 km and 5000 km, and with microturbulent velocities of 5 km s⁻¹, 15 km s⁻¹, and 20 km s⁻¹ (*i.e.* increasing with temperature). These models are static because there is no Doppler brightening effect (DBE) in the He I D₃ line (the photospheric spectrum around the He I D₃ line is flat, *i.e.* continuum), and we neglect the velocity effects on the electron density. The DBE is discussed in Heinzel and Rempel (1987). The helium abundance is fixed at 0.1. The non-LTE code provides the total energy emitted in the helium D₃ line E_{D_3} , the maximum intensity of the He I D₃ profile I_0 , the mean electron density n_e , as well as the optical thickness at the line center of the He I D₃ line $\tau_0(D_3)$. We note that radiative-transfer codes have been used for the first time to model hot prominence structures inside CMEs.

Our initial analysis revealed that the He I D₃ line is formed mainly under two different regimes, namely through scattering of the incident radiation coming from the disk (for models at low temperatures and low pressures), or by collisional excitation (for models with high temperatures or high pressures). This is in line with the analysis of Labrosse and Gouttebroze (2004). In order to determine the optimal filter around the He I D₃ line for the ASPIICS coronagraph, it is sufficient to select only a subset of our grid of 90 models. Therefore, we present detailed results only for three temperature models: 8 kK, 30 kK, and 100 kK. These correspond to three cases of prominence ejecta that can be observed by the ASPIICS coronagraph – cool, warm, or hot prominence material in the corona. We note that the latter was identified as a prominence flux-rope in the core of the CME emitting in hydrogen Lyman lines and other hotter lines (Heinzel *et al.*, 2016; Jejič *et al.*, 2017). At 8 kK, the He I D₃ line formation is dominated by scattering of the incident radiation in the He I D₃ line. At the two higher temperatures, collisional processes will dominate. In particular, all models at 30 kK show maximum emission in the He I D₃ line: at temperatures higher than 30 kK, neutral helium starts to be noticeably ionized, and

Table 1 Temperature T , microturbulent velocity ξ , mean electron density n_e , integrated intensity emitted in the He I D₃ line E_{D_3} , optical thickness at the line center of the He I D₃ line $\tau_0(D_3)$, and optical thickness of VL τ_{VL} for three representative non-LTE models. The models have fixed gas pressure $p = 0.1 \text{ dyn cm}^{-2}$, thickness $D = 1000 \text{ km}$, and height above the solar surface $h = 60 \text{ Mm}$.

Model	T (kK)	ξ (km s ⁻¹)	n_e (10 ¹⁰ cm ⁻³)	E_{D_3} (erg s ⁻¹ cm ⁻² sr ⁻¹)	$\tau_0(D_3)$ (10 ⁻³)	τ_{VL} (10 ⁻⁷)
1	8	5	2.16	657.5	2.40	14.4
2	30	15	1.26	2237.9	3.50	8.4
3	100	20	0.378	8.4	0.01	2.5

the intensity of the emerging He I D₃ line decreases with temperature. For this study, all other input parameters are fixed to one set of values: an altitude above the limb of 60 Mm, a gas pressure of 0.1 dyn cm⁻², and a slab thickness of 1000 km. The microturbulent velocity is taken to be 5 km s⁻¹ at $T = 8 \text{ kK}$, 15 km s⁻¹ at $T = 30 \text{ kK}$, and 20 km s⁻¹ at $T = 100 \text{ kK}$ (see Table 1). A more detailed analysis of the He I D₃ line intensity and how it will be observed in the ASPIICS filter will be presented in a follow-up paper (Labrosse, Jejčič, and Heinzel, 2018).

4. Visible-Light Emission

The integrated VL intensity of a prominence E_{VL} is due to Thomson scattering of the solar incident radiation on free electrons in the prominence plasma and depends on n_e and D ,

$$E_{VL} = \sigma_T W(h, \lambda_c) I_{\text{tot}} n_e D. \quad (1)$$

VL emission is thus proportional to the column electron density $N_e = n_e D$. Here σ_T is the Thomson scattering cross section. We note that the optical thickness is $\tau_{VL} = \sigma_T n_e D$ (see Table 1). $W(h, \lambda_c)$ is the dilution factor, which depends on the height above the solar surface and on the central wavelength of the filter due to the limb darkening of incident radiation. Jejčič and Heinzel (2009; see Appendix therein) showed the height and wavelength dependence of the dilution factor in the optical range up to an altitude of 100 Mm. Here we are interested in VL emission around the He I D₃ line, and thus the wavelength of the He I D₃ line center is used. I_{tot} (see Table 2) has to be computed in the wavelength range in which the VL is detected,

$$I_{\text{tot}} = \int I_0(\lambda) G(\lambda) d\lambda. \quad (2)$$

Here $I_0(\lambda)$ is the VL continuum photospheric intensity at a given wavelength using the data from Allen (1973) and $G(\lambda)$ is the Gaussian-shaped filter transmittance around the He I D₃ line with an FWHM equal to 5, 10, and 20 Å for narrow-band filters, or a uniform transmittance for a 300 Å broad-band VL filter between 5400 and 5700 Å and a narrow-band flat filter with a width of 20 Å (see Section 2). For the three representative models discussed in Section 3, VL emission is computed using Equation 1, and the results are presented in Table 2 for all studied filters.

The ASPIICS coronagraph will detect the mixture of the He I D₃ and VL contributions through the narrow-band filter,

Table 2 Computed values of VL intensities I_{tot} and integrated VL emissions E_{VL} for different filters and for three representative prominence models presented in Table 1.

Filter FWHM (Å)	Flat	Gaussian		Broad-band	
	20	5	10	20	300
I_{tot} ($10^7 \text{ erg s}^{-1} \text{ cm}^{-2} \text{ sr}^{-1}$)	6.46	1.72	3.43	6.87	101.44
E_{VL} (#1) ($\text{erg s}^{-1} \text{ cm}^{-2} \text{ sr}^{-1}$)	21.76	5.79	11.58	23.15	335.90
E_{VL} (#2) ($\text{erg s}^{-1} \text{ cm}^{-2} \text{ sr}^{-1}$)	12.69	3.38	6.75	13.51	195.94
E_{VL} (#3) ($\text{erg s}^{-1} \text{ cm}^{-2} \text{ sr}^{-1}$)	3.81	1.01	2.03	4.05	58.78

$$E_{\text{tot}}(\text{nb}) = E_{\text{D3}}(\text{nb}) + E_{\text{VL}}(\text{nb}). \tag{3}$$

Here we use (nb) for a narrow-band filter to clearly distinguish it from the broad-band (bb) filter. Since the instrument will make quasi-simultaneous images in the broad-band VL filter, the pure helium image and the pure VL image of the prominence can be reconstructed. VL emission in the broad-band filter can be written in the same way as in the narrow-band filter (see Equations 1 and 2). If the broad-band and narrow-band intensities are calibrated in absolute units, we obtain

$$E_{\text{VL}}(\text{nb}) = E_{\text{VL}}(\text{bb}) \frac{W(h, \lambda_{\text{nb}}) \int I_0(\lambda) G_{\text{nb}}(\lambda) d\lambda}{W(h, \lambda_{\text{bb}}) \int I_0(\lambda) G_{\text{bb}}(\lambda) d\lambda} = E_{\text{VL}}(\text{bb})\alpha, \tag{4}$$

where α is a known parameter for a given height through the dilution factors that depend on the filter (for nb we take the wavelength of the He I D₃ line, and for bb we take 5550 Å) and filter transmittance shape. The pure He I D₃ contribution in the narrow-band filter can be then written as

$$E_{\text{D3}}(\text{nb}) = E_{\text{tot}}(\text{nb}) - E_{\text{VL}}(\text{nb}). \tag{5}$$

5. Visibility of the He I D₃ Prominence Structures with the ASPICs Coronagraph

Figure 1 shows the effect of the LOS velocity 300 km s^{-1} on the prominence He I D₃ line due to the filter transmission curves at four different narrow-band filters. The narrow-band 20 Å flat filter is marked in brown, and the three Gaussian filters have the following color-coding: blue for 5 Å, green for 10 Å, and red for 20 Å. This color-coding is used for all following plots. For the He I D₃ line, the Doppler shift of 1 Å roughly corresponds to an LOS velocity of 50 km s^{-1} . This plot clearly shows that at large Doppler shifts of the prominence structure, only the flat filter will transmit the whole signal of the He I D₃ line, while Gaussian filters will reduce the signal by a certain factor. At this rather extreme LOS velocity, the helium signal would be reduced by about 20% in case of the 20 Å filter, by about 60% in case of the 10 Å filter, and it is practically completely reduced by the 5 Å filter. This demonstrates that the optimal choice would be the 20 Å flat narrow-band filter. A possible option is a design of the 20 Å narrow-band filter with transmittance between a flat and a Gaussian shape.

Figure 2a shows the variation of the integrated intensity emitted in the He I D₃ line with temperature for four narrow-band filters and three LOS velocities for the three prominence models shown in Table 1. We chose two representative LOS velocities, 100 and 300 km s^{-1} , according to our previous experiences with fast-moving prominence structures (Heinzl

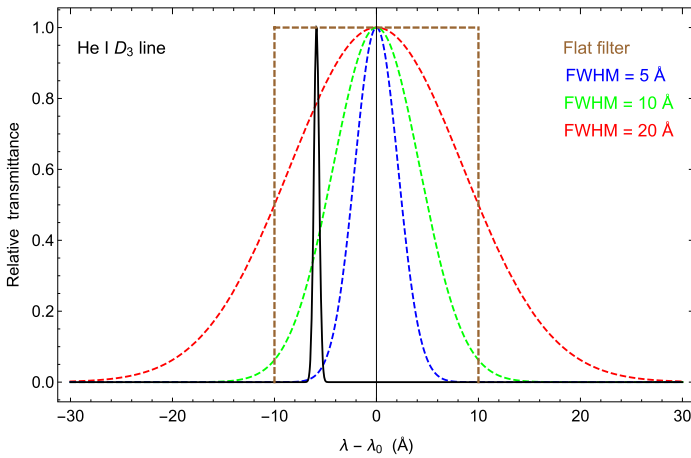


Figure 1 Transmittance normalized to the peak values as a function of wavelength around the He I D₃ line for all four studied narrow-band filters together with the Doppler-shifted He I D₃ profile at an LOS velocity of 300 km s⁻¹.

et al., 2016), and we added a zero velocity as the reference for static prominence structures. E_{D_3} is highest for warm prominence structures at 30 kK and lowest for the hot prominence model at 100 kK, where the helium is almost fully ionized. The flat filter is a reference filter that gives the correct energy emitted in the He I D₃ line because the filter transmittance is uniform. By increasing the prominence LOS velocity from 0 up to 300 km s⁻¹, the energy detected in the He I D₃ line is decreasing for narrower Gaussian filters. The difference between the flat and Gaussian filter is highest at 5 Å and lowest at 20 Å.

By separating the integrated intensity of the He I D₃ line and the prominence VL emission using the broad-band filter as described in Section 4, we can reconstruct similar plot as in Figure 2a. Figure 2b shows the ratio of the integrated intensity emitted in the He I D₃ line to the prominence VL emission as a function of temperature for representative models. The ratios are presented in Table 3. Because both the He I D₃ and the narrow-band VL emissions are optically thin (see Table 1), their ratio is independent of the prominence thickness, meaning that it may provide a useful diagnostic of the temperature. For a given range of prominence LOS velocities and narrow-band filters, the ratio of the energy that is emitted in the He I D₃ line to the VL emission is between 0.1 and 10 for hot prominence structures, between 1 and 100 for cool structures, and between 10 and 1000 for warm structures. Figure 3 shows the effect of various filters and the prominence LOS velocities on the integrated intensity of the He I D₃ line and the VL emission. The plot clearly shows that for lower LOS velocities 0, and 100 km s⁻¹, the contrast of the He I D₃ line with respect to the prominence VL emission is decreasing with the filter width, while for higher LOS velocities of 300 km s⁻¹, the contrast is increasing with the filter width (see connecting lines). In order to be able to detect fast-moving structures, we must find a compromise between the filter that will compose the broadest range of LOS velocities and the width that provides the best detectability of the He I D₃ emission. The majority of points in Figure 3 lie above the diagonal, which indicates a good detectability of the He I D₃ line emission. For the range of prominence LOS velocities up to 300 km s⁻¹, the Gaussian filter with 20 Å FWHM gives the closest values to the flat filter, which indicates that a real design of the narrow-band filter centered on the He I D₃ line should be the 20 Å flat filter or somewhere between the flat and Gaussian filter with an FWHM of 20 Å.

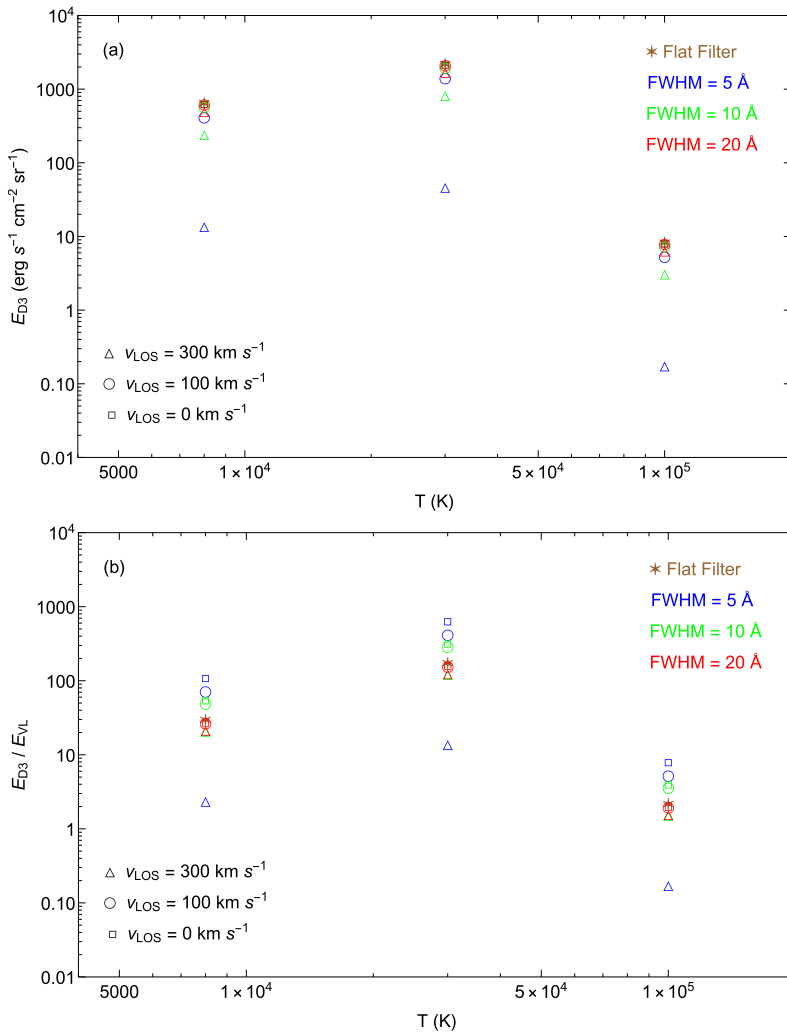


Figure 2 **a)** Integrated intensity emitted in the He I D₃ line as a function of temperature for the models shown in Table 1. **b)** Ratio of the integrated intensity emitted in the He I D₃ line to the VL emission as a function of temperature for the models.

6. Contamination with the Na I D₁ and D₂ Lines and the Comet Detection Capability of ASPIICS

The sodium doublet Na I D₁ and D₂ at 5897.56 and 5891.58 Å lies close to the He I D₃ line and may contaminate the signal for fast-moving prominence structures. If the narrow-band filter is wide enough, the sodium lines can be well detected in comets passing through the ASPIICS FOV, which represents an interesting option for ASPIICS.

The magnitude of comets observed in VL coronagraphs is not only due to photospheric light scattered by dust grains, but also to emission processes by neutrals or singly ionized atoms. In particular, a distinct neutral sodium tail has been reported for many comets

Table 3 Ratio of integrated intensity emitted in the He I D₃ line to the prominence VL emission for different prominence LOS velocities and models. For Gaussian filters, the FWHMs are presented.

Filter	Flat 20 Å	Gaussian 5 Å	Gaussian 10 Å	Gaussian 20 Å
v_{LOS} (km s ⁻¹)		Model 1		
0	30.22	113.57	56.80	28.40
100		74.22	51.07	27.65
300		2.47	21.81	22.36
v_{LOS} (km s ⁻¹)		Model 2		
0	176.31	662.66	331.43	165.70
100		433.04	297.99	161.36
300		14.40	127.26	130.44
v_{LOS} (km s ⁻¹)		Model 3		
0	2.21	8.29	4.15	2.07
100		5.42	3.73	2.02
300		0.18	1.59	1.63

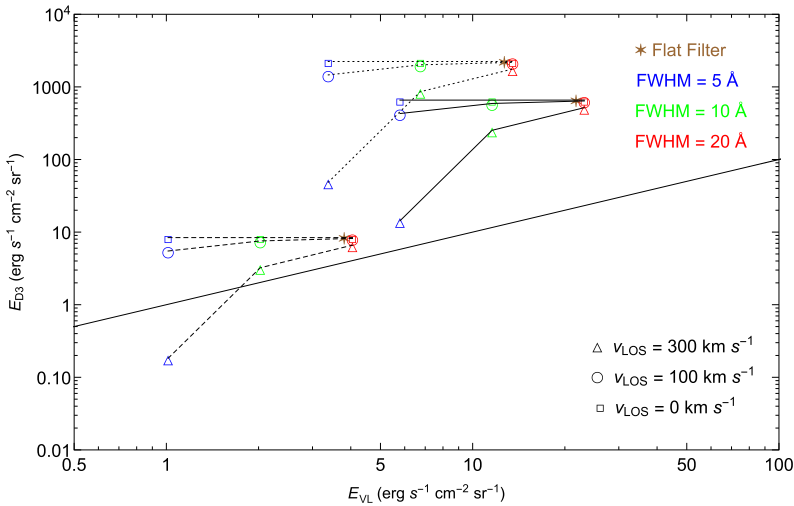


Figure 3 Integrated intensity of the He I D₃ line as a function of VL emission for selected models. Model 1 is presented with a *solid line*, model 2 with a *dotted line*, and model 3 with a *dashed line*. We show the effect of various filters and the prominence LOS velocities. The *straight black solid line* shows where $E_{\text{D}_3} = E_{\text{VL}}$.

(Biesecker *et al.*, 2002). Strong Na I emission at small heliocentric distances has been detected in many comets (*e.g.* comet Ikeya–Seki, Preston 1967, Slaughter 1969), and a distinct Na I tail was first imaged by Cremonese *et al.* (1997) at comet Hale–Bopp (C/1995 O1). This emission is very bright thanks to the high efficiency of the sodium D transition (see *e.g.* Cremonese 1999 for a discussion of the origin of the sodium tail). The sodium tail is in addition to the two most common dust and ion tails, and it is responsible for the significant differences in the apparent comet magnitudes depending on the band-pass filter used for

coronagraphic observations, as discussed by Knight *et al.* (2010). This brightness increase (by about a factor 10) is relatively more important for “narrow-band” (such as the “orange” LASCO-C2 and LASCO-C3 filters, 5400–6400 Å) than for broad-band (such as the “clear” LASCO-C3 filter, 4000–8500 Å) filters, and is most likely due to the sodium D₁ and D₂ lines, even if contributions from other lines by other atoms or ions cannot be excluded. Significant differences have been observed for instance between light curves for the same comet (ISON C/2012 S1) observed with the LASCO and STEREO coronagraphs (Knight and Battams, 2014), and these differences are related mostly to the fact that the bandpasses for the COR1 (6500–6600 Å) and COR2 (6500–7500 Å) coronagraphs do not include the sodium lines.

As reported by Biesecker *et al.* (2002), the majority of Sun-grazing comets usually disappear below heliocentric distances of about $7 R_{\odot}$, hence no emission from these comets is expected in the ASPIICS FOV. Nevertheless, recent spectacular observations of near-Sun comets (such as ISON C/2012 S1) and Sun-grazing comets (such as Lovejoy C/2011 W3) demonstrate that similar objects could fall in the ASPIICS FOV and even survive at their perihelion transit. In particular, during the transit of comet ISON, it was demonstrated for the first time that similar comets can be observed in VL coronagraphs imaging the inner corona even from the ground (Druckmüller *et al.*, 2014). Hence, the inclusion of the D₁ and D₂ lines in the future ASPIICS He I D₃ band-pass filter centered on 5877.25 Å could allow similar observations for future comets. Nevertheless, this would imply broad band-passes that are up to 28 Å and 40 Å wide to include the sodium D₁ and D₂ lines, respectively.

Effects due to the cometary orbital motion should be considered as well. The cometary emission from sodium atoms will in general be Doppler shifted if the comet has a significant projected velocity along the LOS that might in general be directed either toward the observer or away from the observer. The maximum possible speed for these bodies is equal to the free-fall speed, which, by assuming a heliocentric perihelion distance of $1.2 R_{\odot}$, for instance, is about 560 km s^{-1} , corresponding to a maximum expected Doppler shift of about 11 Å. The sodium atoms expelled from the comet will undergo radiation pressure acceleration in the anti-sunward direction, hence these atoms will likely move at a speed lower than the cometary orbital speed. In any case, by assuming an He I band-pass filter centered on 5877.25 Å with a full-width of 20 Å, the cometary sodium emission at 5891.58 and 5897.56 Å will start to fall in the band-pass only for Doppler blueshifts higher than 4 Å and 10 Å, corresponding to velocities higher than 200 km s^{-1} and 500 km s^{-1} . In summary, cometary sodium emission will likely fall outside the narrow-band He I D₃ filter, unless much broader band-passes are chosen. This will significantly reduce the detection probability of comets with this filter, because sodium lines will fall in the filter band-pass only for significant Doppler blueshifts, which are possible but quite unlikely. Nevertheless, bright comets will also be observed by ASPIICS with the VL filters (5400–5700 Å), providing nice imaging of the dust tails in the inner corona, and might even be observed in the “green line” filter, as recently demonstrated by the AIA observations of comet Lovejoy (McCaughey *et al.*, 2013). Hence, by considering that the He I D₃ filter is designed primarily to perform scientific observations of solar prominences, this probable loss of detection capability of comets can be considered acceptable.

To study the possible contribution of sodium Na I D₁ and D₂ lines in prominences observed by the narrow-band He I D₃ filter, we used the spectra obtained in the past on photographic plates at the Ondřejov Observatory. These spectra contain many prominences observed in the He I D₃ and the sodium D₁ and D₂ lines. Photographic densities were converted into relative intensities with standard procedure using a calibration wedge (Valníček *et al.*, 1959). The photospheric scattered light was subtracted. An example where the contribution of sodium D₁ and D₂ lines in prominences is negligible compared to the He I D₃ line is

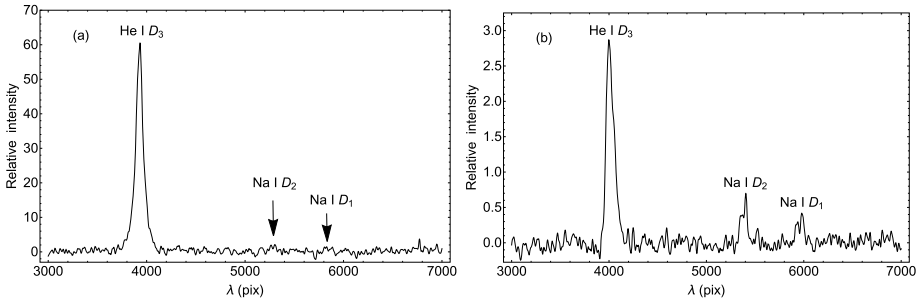


Figure 4 a) Example of measured profiles of the He I D₃ and the Na I D₁ and D₂ lines. Contribution of Na I D₁ and D₂ lines is negligible. b) Contribution of Na I D₁ and D₂ lines is between 10 and 15% with respect to the He I D₃ line.

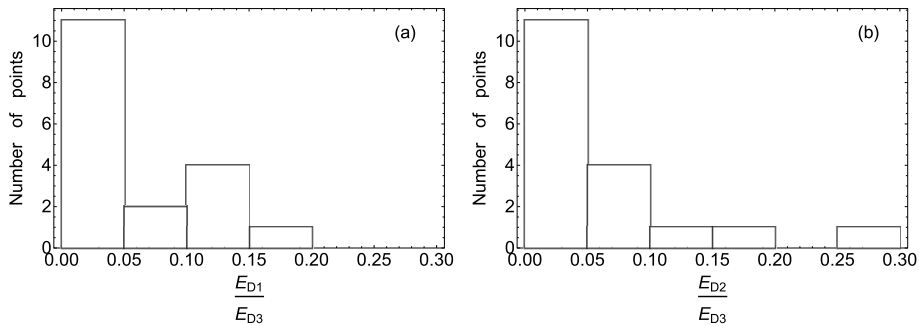


Figure 5 a) Distribution of the energy ratio emitted in the Na I D₁ line to the He I D₃ line. b) Distribution of energy ratio emitted in the Na I D₂ line to the He I D₃ line.

shown in Figure 4a, while Figure 4b shows an example where the contribution of the sodium D₁ and D₂ lines in the prominence is important.

We analyzed 18 prominence spectra from Ondřejov Observatory in total. The results are presented as histograms in Figure 5, showing the relative brightness contribution of the Na I D₁ and Na I D₂ lines *versus* the He I D₃ line. The histograms show that peak is below 5%. These are mostly quiescent prominences; in bright quiescent prominences, the ratio can increase to 10%. These results are consistent with the work of Stellmacher and Wiehr (2005), who obtained similar results for the Na I D₂ line. Only in a few cases is the ratio between Na I D₁ and He I D₃ or Na I D₂ and He I D₃ higher than 20%. These extreme cases seem to be related to the DBE in the sodium D₁ and D₂ lines. The sodium doublet is very sensitive to DBE because these photospheric absorption lines are very deep and relatively narrow.

It is important to know how much each line contributes to the narrow-band filter signal to determine how important the Na I D₁ and D₂ lines are compared to the He I D₃ line and how their ratio depends on the filter width. To do this, we made two examples with a Gaussian narrow-band filter with an FWHM equal to 20 and 30 Å. In Table 4 we list the relative contribution of the Na I D₁ and D₂ lines and the He I D₃ line to the filter signal at an upper limit of the radial flow velocity $v_{\text{rad}} = 450 \text{ km s}^{-1}$ (which takes into account DBE on the sodium D₁ and D₂ lines) for three different prominence LOS velocities of 0, 100, and 300 km s⁻¹ moving in two directions: toward the observer (blueshift) or away from the

Table 4 Total energy emitted in the Na I D₁ and D₂ lines with respect to the energy emitted in the He I D₃ line at the upper limit of a radial flow velocity of 450 km s⁻¹ and for various LOS velocities at blueshift and redshift.

FWHM (Å)	v_{rad} (km s ⁻¹)	v_{LOS} (km s ⁻¹)	$\frac{E_{D_2}+E_{D_1}}{E_{D_3}}$ Blueshift	$\frac{E_{D_2}+E_{D_1}}{E_{D_3}}$ Redshift
20	450	0	0.036	0.036
		100	0.055	0.024
		300	0.128	0.010
30	450	0	0.095	0.095
		100	0.116	0.078
		300	0.172	0.053

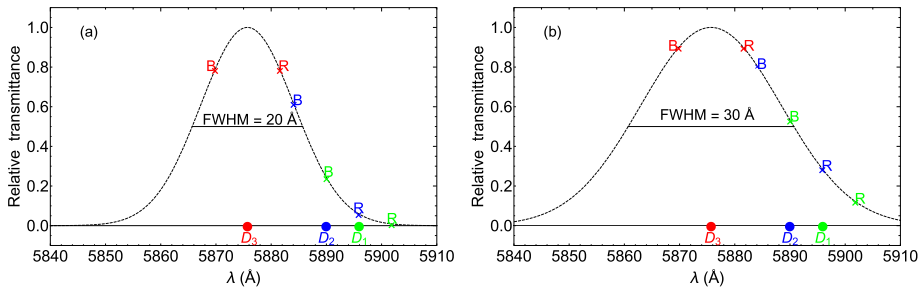


Figure 6 **a)** Contamination of the Gaussian 20 Å narrow-band filter with the Na I D₁ and D₂ lines at an LOS velocity ± 300 km s⁻¹. The He I D₃ line is plotted in red, the Na I D₁ and D₂ lines in green and blue. Crosses show the position of all three lines at the given LOS velocities. R stands for redshift and B for blueshift. **b)** Contamination of the Gaussian 30 Å narrow-band filter with the Na I D₁ and D₂ lines at LOS velocities ± 300 km s⁻¹.

observer (redshift) for two filter widths. In the 20 Å filter the contributions of the Na I D₁ and D₂ lines and VL are almost negligible, a prominence will be well visible in He I D₃, the exception is an extreme case with about 13% of Na I D₁ and D₂ contamination. With the 20 Å wide He I D₃ filter, ASPIICS can only detect comets in the Na I D₁ and D₂ lines if they move with an LOS velocity of 300 km s⁻¹ or higher toward the observer (see Figure 6a). In the 30 Å Gaussian filter the prominence VL emission brightness increases, which would lower the He I D₃ line contrast. For the 30 Å wide filter, the VL emissions of models 1, 2, and 3 are 34.68, 20.23, and 6.07 erg s⁻¹ cm⁻² sr⁻¹. If there is no LOS motion of the prominence, we automatically obtain about 10% of the emission from the Na I D₁ and D₂ lines through the filter. At an LOS velocity of 300 km s⁻¹ (see Figure 6b), we obtain 17% of Na I D₁ and D₂ lines at blueshift, which is a not negligible contribution, and 5% at redshift. In the 30 Å filter the prominence would be more contaminated by the Na I D₁ and D₂ lines and prominence VL emission. However, for this filter, comets will be better detected, while prominences will be more highly contaminated with the Na I D₁ and D₂ contribution. Our analysis therefore shows that a 20 Å filter will provide an optimal detectability of the He I D₃ line in eruptive prominences.

7. Conclusions

We investigated the properties of an optimal narrow-band filter centered on the neutral helium He I D₃ line at 5877.25 Å for eruptive prominence and CME observations down to 1.08 R_⊙ (60 Mm) with the ASPIICS coronagraph onboard the satellite PROBA-3. We studied the expected visibility of prominences through various narrow-band filters in the ASPIICS coronagraph. This depends on the filter transmittance profile and on the physical conditions in the prominences. We took into consideration four narrow-band filters: three Gaussian filters with an FWHM equal to 5, 10, and 20 Å, and one 20 Å flat filter. A narrow-band He I D₃ filter mainly contains the radiation contribution from the prominence He I D₃ line and prominence VL emission. The modeled prominence He I D₃ line emission was computed with a multilevel 1D non-LTE code for helium, and the emerging line profiles were multiplied by the narrow-band filter transmittance. The integrated VL emission in prominences was also computed for all four narrow-band filters. We presented several relations between the prominence He I D₃ line emission and the prominence VL emission depending on three typical prominence LOS (Doppler) velocities: 0, 100, and 300 km s⁻¹ in a given narrow-band filter. We selected three representative prominence models with temperatures 8 kK (cool prominence structures), 30 kK (warm structures), and 100 kK (hot structures). These relations show i) the maximum emission in the He I D₃ line at 30 kK and the minimum emission at 100 kK, ii) by increasing the prominence LOS velocity, E_{D_3} decreases when the Gaussian filter is narrowed, iii) the contrast of E_{D_3} with respect to E_{VL} for lower LOS velocities 0 and 100 km s⁻¹ decreases with increasing filter width, while it increases at 300 km s⁻¹, and finally, iv) E_{D_3}/E_{VL} can provide a useful diagnostic for the temperature of prominence structures. Models show that this ratio (which depends on the prominence LOS velocity and filter width) is between 0.1 and 10 for hot prominence structures, between 1 and 100 for cool structures, and between 10 and 1000 for warm structures. The He I D₃ filter will produce a mixture of He I D₃ line emission and VL emission (at a given wavelength position of the filter transmittance profile), therefore we can reconstruct the pure helium image of the prominence, as well as the pure VL image thanks to the simultaneous broad-band VL continuum observations, but without any information about the prominence LOS velocities. We also showed the possible contamination of the signal with the nearby sodium doublet Na I D₁ and D₂ in 20 and 30 Å Gaussian filters. Our recommendation is to design a narrow-band 20 Å flat filter or a filter somewhere between flat and Gaussian with an FWHM of 20 Å. This is mainly dictated by the lack of information about the prominence LOS velocity. However, a 30 Å filter (flat or almost flat) would suit the expected cometary detections in Na I lines better. A filter like this will degrade the He I D₃ prominence contrast more strongly, but He I D₃ will still be higher than or comparable to the VL emission. As we have shown, the prominence images in He I D₃ and VL can be separated using the broad-band VL filter data, but the 30 Å filter signal will be more strongly contaminated by prominence sodium lines (Figure 6), and this contribution cannot be separated. A 20 Å filter centered off-band of He I D₃ toward the red was also an option, but then the bluishifted prominences would be less well detectable. A more detailed analysis of the He I D₃ line, its diagnostics, and how it will be observed with the ASPIICS filter will be presented in our next paper (Labrosse, Jejič, and Heinzel, 2018).

Acknowledgements SJ acknowledges the financial support from the Slovenian Research Agency No. P1-0188. SJ, PH, and SG acknowledge support from the Czech Funding Agency through grant No. 16-18495S and from the AIAS through RVO-67985815. NL acknowledges support from STFC grant ST/L000741/1. NL, PH, and SG also acknowledge support by the International Space Science Institute (ISSI), and through the Team of NL that studies solar prominences. ANZ acknowledges support from the Belgian Federal Science

Policy Office through the ESA-PRODEX programme (grant No. 4000117262). SG and PH acknowledge the support from grant 16-17586S of the Czech Science Foundation. The Ondřejov archive spectra were digitized by Alicja Heinzl. The authors thank the anonymous referee for valuable comments and suggestions.

Disclosure of Potential Conflicts of Interest The authors declare that they have no conflicts of interest.

References

- Allen, C.W.: 1973, *Astrophysical Quantities*, Athlone Press, London, 172.
- Bemporad, A., Poletto, G., Raymond, J., Giordano, S.: 2007, A review of SOHO/UVCS observations of sungrazing comets. *Planets* **55**, 1021. DOI.
- Biesecker, D.A., Lamy, P., St. Cyr, O.C., Llebaria, A., Howard, R.A.: 2002, Sungrazing comets discovered with the SOHO/LASCO coronagraphs 1996–1998. *Icarus* **157**, 323. DOI.
- Boulade, S., Delannée, C., Koutchmy, S., Lamy, P., Llebaria, A., Howard, R., Schwenn, R., Simnett, G.: 1997, Analysis of a high latitude slow CME with travelling ejecta. In: Wilson, A. (ed.) *Fifth SOHO Workshop: The Corona and Solar Wind Near Minimum Activity*, ESA Special Publication **404**, 217.
- Brueckner, G.E., Howard, R.A., Koomen, M.J., Korendyke, C.M., Michels, D.J., Moses, J.D., Socker, D.G., Dere, K.P., Lamy, P.L., Llebaria, A., Bout, M.V., Schwenn, R., Simnett, G.M., Bedford, D.K., Eyles, C.J.: 1995, The Large Angle Spectroscopic Coronagraph (LASCO). *Solar Phys.* **162**, 357. DOI.
- Cremonese, G.: 1999, Hale-Bopp and its sodium tails. *Space Sci. Rev.* **90**, 83. DOI.
- Cremonese, G., Boehnhardt, H., Crovisier, J., Rauer, H., Fitzsimmons, A., Fulle, M., Licandro, J., Pollacco, D., Tozzi, G.P., West, R.M.: 1997, Neutral sodium from comet Hale-Bopp: a third type of tail. *Astrophys. J. Lett.* **490**, L199. DOI.
- Druckmüller, M., Habbal, S.R., Aniol, P., Ding, A., Morgan, H.: 2014, Imaging comet ISON C/2012 S1 in the inner corona at perihelion. *Astrophys. J. Lett.* **784**, L22. DOI.
- Heinzl, P., Rimpolt, B.: 1987, Hydrogen emission from moving solar prominences. *Solar Phys.* **110**, 171. DOI.
- Heinzl, P., Susino, R., Jejič, S., Bemporad, A., Anzer, U.: 2016, Hot prominence detected in the core of a coronal mass ejection: analysis of SOHO/UVCS $L\alpha$ and SOHO/LASCO visible-light observations. *Astron. Astrophys.* **589**, A128. DOI.
- Howard, R.A., Moses, J.D., Vourlidas, A., Newmark, J.S., Socker, D.G., Plunkett, S.P., Korendyke, C.M., Cook, J.W., Hurley, A., Davila, J.M., Thompson, W.T., St. Cyr, O.C., Mentzell, E., Mehalick, K., Lemen, J.R., Wuelsel, J.P., Duncan, D.W., Tarbell, T.D., Wolfson, C.J., Moore, A., Harrison, R.A., Waltham, N.R., Lang, J., Davis, C.J., Eyles, C.J., Mapson-Menard, H., Simnett, G.M., Halain, J.P., Defise, J.M., Mazy, E., Rochus, P., Mercier, R., Ravet, M.F., Delmotte, F., Auchere, F., Delaboudiniere, J.P., Bothmer, V., Deutsch, W., Wang, D., Rich, N., Cooper, S., Stephens, V., Maahs, G., Baugh, R., McMullin, D., Carter, T.: 2008, Sun Earth Connection Coronal and Heliospheric Investigation (SECCHI). *Space Sci. Rev.* **136**, 67. DOI.
- Jejič, S., Heinzl, P.: 2009, Electron densities in quiescent prominences derived from eclipse observations. *Solar Phys.* **254**, 89. DOI.
- Jejič, S., Susino, R., Heinzl, P., Džifčáková, E., Bemporad, A., Anzer, U.: 2017, Hot prominence detected in the core of a coronal mass ejection: II. Analysis of CIII line detected by SOHO/UVCS. *Astron. Astrophys.* **607**, A80. DOI.
- Knight, M.M., Battams, K.: 2014, Preliminary analysis of SOHO/STEREO observations of sungrazing comet ISON (C/2012 S1) around perihelion. *Astrophys. J. Lett.* **782**, L37. DOI.
- Knight, M.M., A'Hearn, M.F., Biesecker, D.A., Fauray, G., Hamilton, D.P., Lamy, P., Llebaria, A.: 2010, Photometric study of the Kreutz comets observed by SOHO from 1996 to 2005. *Astron. J.* **139**, 926. DOI.
- Kohl, J.L., Esser, R., Gardner, L.D., Habbal, S., Daigneau, P.S., Dennis, E.F., Nystrom, G.U., Panasyuk, A., Raymond, J.C., Smith, P.L., Strachan, L., van Ballegoijen, A.A., Noci, G., Fineschi, S., Romoli, M., Ciaravella, A., Modigliani, A., Huber, M.C.E., Antonucci, E., Benna, C., Giordano, S., Tondello, G., Nicolosi, P., Naletto, G., Pernechele, C., Spadaro, D., Poletto, G., Livi, S., von der Lühe, O., Geiss, J., Timothy, J.G., Gloeckler, G., Allegra, A., Basile, G., Brusa, R., Wood, B., Siegmund, O.H.W., Fowler, W., Fisher, R., Jhabvala, M.: 1995, The ultraviolet coronagraph spectrometer for the Solar and Heliospheric Observatory. *Solar Phys.* **162**, 313. DOI.
- Labrosse, N.: 2015, Derivation of the major properties of prominences using NLTE modelling. In: Vial, J.-C., Engvold, O. (eds.) *Solar Prominences, Astrophysics and Space Science Library* **415**, 131. DOI.
- Labrosse, N., Gouttebroze, P.: 2001, Formation of helium spectrum in solar quiescent prominences. *Astron. Astrophys.* **380**, 323. DOI.

- Labrosse, N., Gouttebroze, P.: 2004, Non-LTE radiative transfer in model prominences. I. Integrated intensities of He I triplet lines. *Astrophys. J.* **617**, 614. [DOI](#).
- Labrosse, N., Ježičič, S., Heinzel, P.: 2018, Prominence diagnostics with ASPIICS, in preparation.
- Lamy, P., Damé, L., Vivès, S., Zhukov, A.: 2010, ASPIICS: a giant coronagraph for the ESA/PROBA-3 formation flying mission. In: *Space Telescopes and Instrumentation 2010: Optical, Infrared, and Millimeter Wave, Proc. SPIE 7731*, 773118. [DOI](#).
- Lamy, P., Fauray, G., Llebaria, A., Knight, M.M., A'Hearn, M.F., Battams, K.: 2013, Sunskirting comets discovered with the LASCO coronagraphs over the decade 1996–2008. *Icarus* **226**, 1350. [DOI](#).
- McCauley, P.I., Saar, S.H., Raymond, J.C., Ko, Y.-K., Saint-Hilaire, P.: 2013, Extreme-ultraviolet and X-ray observations of comet lovejoy (C/2011 W3) in the lower corona. *Astrophys. J.* **768**, 161. [DOI](#).
- Preston, G.W.: 1967, The spectrum of Ikeya–Seki (1965f). *Astrophys. J.* **147**, 718. [DOI](#).
- Renotte, E., Buckley, S., Cernica, I., Denis, F., Desselle, R., De Vos, L., Fineschi, S., Fleury-Frenette, K., Galano, D., Galy, C., Gillis, J.-M., Graas, E., Graczyk, R., Horodyska, P., Kranitis, N., Kurowski, M., Ladno, M., Liebecq, S., Loreggia, D., Mechmech, I., Melich, R., Mollet, D., Mosdorf, M., Mroczkowski, M., O'Neill, K., Patočka, K., Paschalis, A., Peresty, R., Radzik, B., Rataj, M., Salvador, L., Servaye, J.-S., Stockman, Y., Thizy, C., Walczak, T., Zarzycka, A., Zhukov, A.: 2016, Recent achievements on ASPIICS, an externally occulted coronagraph for PROBA-3. In: *Space Telescopes and Instrumentation 2016: Optical, Infrared, and Millimeter Wave, Proc. SPIE 9904*, 99043D. [DOI](#).
- Sekanina, Z.: 2003, Erosion model for the sungrazing comets observed with the Solar and Heliospheric Observatory. *Astrophys. J.* **597**, 1237. [DOI](#).
- Slaughter, C.D.: 1969, The emission spectrum of comet Ikeya–Seki 1965-f at perihelion passage. *Astron. J.* **74**, 929. [DOI](#).
- Stellmacher, G., Wiehr, E.: 2005, Solar prominences with Na and Mg emissions and centrally reversed Balmer lines. *Astron. Astrophys.* **431**, 1069. [DOI](#).
- Thompson, W.T.: 2009, 3D triangulation of a Sun-grazing comet. *Icarus* **200**, 351. [DOI](#).
- Valníček, B., Letfus, V., Blaha, M., Švestka, Z., Seidl, Z.: 1959, The flare spectrograph at Ondřejov. *Bull. Astron. Inst. Czechoslov.* **10**, 149.